CHAPTER 3

Assessing the impact of HIV spike arrangement on antibody avidity

This chapter presents a hypothesis called the "island effect" that may explain the poor efficacy of existing broadly neutralizing anti-HIV antibodies and the ongoing failure to develop a vaccine capable of eliciting any substantial neutralizing antibody response, and data are presented on the development of antibody hinge extension technologies that could eventually lead to novel antibody architectures capable of overcoming this effect. This work was completed with the assistance of Priyanthi Gnanapragasm, Rachel Galimidi, Chris Foglesong, and Maria Suzuki.

Introduction

It is estimated that since 1990, there have been more than 50 million HIV infections (1). Yet despite a well-developed global network of treatment and monitoring facilities, to date, the only documented case in which an established infection was apparently cleared was after complete ablation of the hematopoietic stem cells (HSCs) of an HIV^+ patient undergoing treatment for leukemia followed by replacement with donor HSCs bearing a homozygous deletion of CCR5 (2). Even after HAART-mediated long-term suppression of virus replication to undetectable levels, viral loads eventually rebound after treatment interruption (3), suggesting that it is not possible for a human immune system that has been pre-primed with an infection to enforce HAART-equivalent suppression.

Rapid mutation is a hallmark of HIV infection (4) and is logically invoked as an important factor fueling successful immune evasion that, coupled with the structural features of the envelope trimer, helps explain the paucity of evidence to suggest that the antibody response significantly contributes to the relatively low viral set point observed after the acute viremia phase of infection. Nevertheless, as discussed in previous chapters, conserved epitopes within the envelope trimer have been identified along with broadly neutralizing antibodies (bNAbs) that recognize them. One might predict that passively immunizing an HIV patient by injecting one or more of these bNAbs could lead to indefinite suppression of an infection and/or prevent infection in viral challenge models. Indeed, clinical trials using a cocktail of three bNAbs (2G12, 4E10, and 2F5) demonstrated a partial ability to suppress viral rebound among patients who underwent interruptions in HAART (5). However, the relatively brief delays in viral rebound that

were observed required serum concentrations for the bNAbs totaling ~2 mg/mL. Considering that the volume of blood in a human adult is ~5 liters and that the serum half-lives of most antibodies are at best several weeks, one would need to inject unrealistic quantities of antibodies to achieve even the partial protection seen in this study, where researchers had to inject 1 to 1.3 grams of each antibody weekly (6). The short-lived delay in viral rebound was particularly surprising given the fact that the serum concentrations of each of the individual antibodies ranged up to two orders of magnitude higher than the *in vitro* IC_{90} values for the patients' autologous viruses.

Another study that highlighted the poor performance of bNAbs examined the concentrations required to protect rhesus macaques from infection using chimeric SIV/HIV ($SHIV_{SF162P3}$) derived from strain SF162, which is exceptionally sensitive to the antibody b12 (7), exhibiting an *in vitro* IC_{50} of less than 0.1 μg/mL. Complete protection for these animals from infection by the chimeric virus was observed for dosages at 25 mg/kg, which yielded serum concentrations of approximately 0.7 mg/mL. The concentration of IgG in humans is ~10 mg/mL (8); thus, ~7 % of the total serum IgG would need to be composed of b12 in order to achieve protection against a variant of HIV that was shown to be 50 times more sensitive than the median to b12 among a panel of 19 strains (Fig. 1). These results suggest that if one were to select a typical strain of HIV for the infection challenge, it would probably be necessary to inject enough b12 to more than double the total concentration of IgG in order to achieve protection.

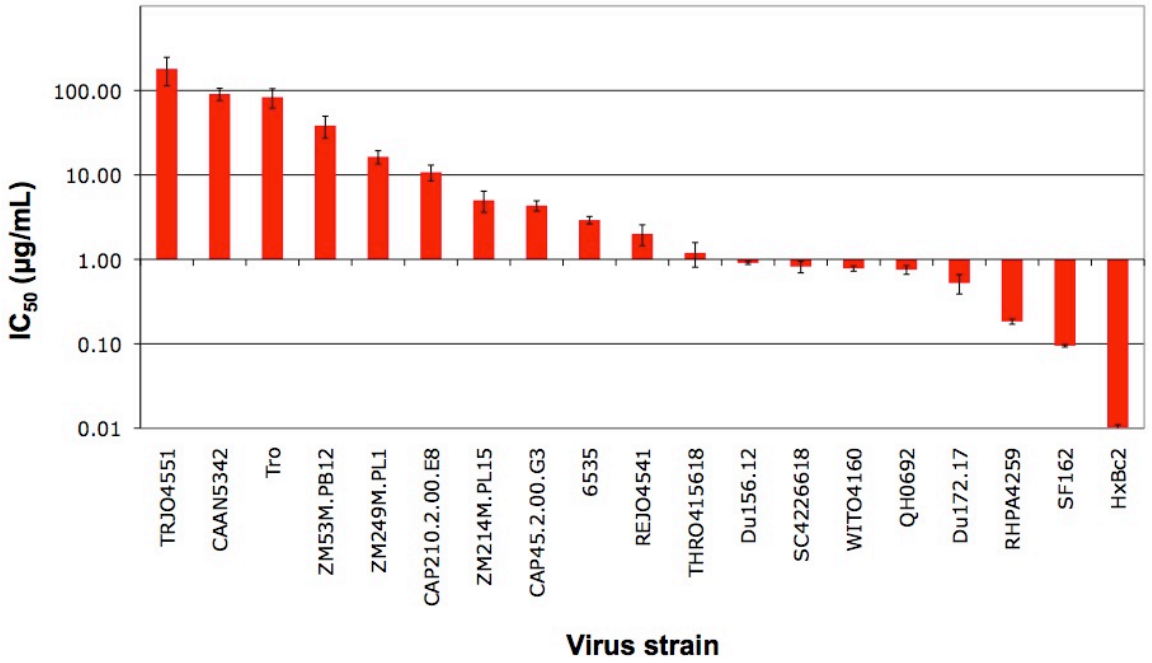

Figure 1. IC_{50} values for the neutralization of various strains of HIV from clades B and C using b12 including SF162, second bar from the right (Klein JS, Gnanapragasm PNP, Björkman PJ, unpublished).

The biophysics of antibody-antigen interactions

The mediocre antibody performance observed in both the human and NHP studies against strains of virus that are unusually sensitive to them suggest that an alternative explanation to rapid mutation may be undermining the capacity of these antibodies to neutralize HIV. To explore this possibility, it is worthwhile to review the structural and biophysical aspects of antibody-antigen interactions.

Intrinsic (*i.e.*, monovalent) antibody-antigen binding mechanisms can often be described using a simple one-step binding model. Consider the interaction between an anti-gp120 Fab and monomeric gp120. In this interaction the Fab, *A*, binds to gp120, *B*, to form a reversible complex, *AB,* which can be described with single rate constants for the forward and reverse reactions, k_1 and k_{-1}:

$$A + B \underset{k-1}{\overset{k1}{\rightleftharpoons}} AB \tag{1}$$

The rate equations that describe the chemical equations can be easily derived from the law of mass action, which states that the rate of any reaction is proportional to the product of the concentration(s) of the reactant(s). Therefore, the instantaneous rates for the formation of *B* and *AB* can be written as:

$$-\frac{d[B]}{dt} = \frac{d[AB]}{dt} = k_1[A][B] - k_{-1}[AB] \tag{2}$$

where [*A*], [*B*], and [*AB*] denote the molar concentrations of the Fab, gp120, and the complex, respectively. This model can be used to derive the intrinsic equilibrium dissociation constant, k_D, which can be calculated from either the ratio of the concentrations of reactants to products when the system is at equilibrium (Eq. 3), or as the ratio of the reverse reaction rate to the forward reaction rate (Eq. 4):

$$k_D = \frac{[A][B]}{[AB]} \tag{3}$$

$$k_D = \frac{k_{-1}}{k_1} \tag{4}$$

In the more complex scenario of binding between one intact bivalent antibody and one stationary envelope spike where intra-spike cross-linking cannot occur (as discussed in Chapter 2), an intrinsic binding model does not account for the effect of having multiple pathways to the formation of the complex, *AB*. Here, binding can occur between the spike and either Fab. Therefore, two equivalent pathways lead to the formation of *AB* and one pathway leads to the formation of *B*, yielding the potential for a two-fold increase in the apparent (*i.e.,* observed) affinity, K_D:

$$K_D = \frac{k_{-1}}{k_1 + k_1} = \frac{k_D}{2} \tag{6}$$

The upper limits of diffusion that have been measured for both Fabs and IgGs, which have been shown to be reduced at distances of up to ~100 nm from planar surfaces and spherical membranes relative to their rates in bulk solution, is between 10^5 and 10^6 $M^{-1}s^{-1}$ (9). Consistent with these findings and the results presented in Chapter 2, values of k_1 for high-affinity antibody-antigen interactions are generally reported to be within the bounds of this upper limit (10-14) despite attempts to develop mutants with enhanced association rates (15). Consequently, in order to achieve mid- to low-picomolar intrinsic affinities, it is necessary for k_{-1} to be $\leq 10^{-4}$ s^{-1} even with the statistical increase in the apparent forward reaction rate that may be observed with the presence of two relatively unconstrained Fab arms.

While antibodies with intrinsic affinities in the nanomolar range are reasonably common, there are few reports of antibodies with intrinsic affinities in the sub-nanomolar

range. However, when both Fab arms are able to engage two binding sites that are fixed in space relative to each other (such as may be observed on the surface of a SPR sensor chip or a pathogen), the resulting increase in apparent affinity can lead to nearly irreversible binding even though the intrinsic affinity may be significantly higher than 1 nM (*e.g.*, see Fig. 2*C* in Chapter 2). This property, called avidity, arises from the relatively low probability that both Fab arms will both occupy a dissociated state for a long enough period of time to allow complete dissociation of the complex. Avidity can be modeled as a two-step binding interaction between a bivalent analyte (the antibody, or *A*) and an immobilized ligand (the antigen, or *B*), which can form the complexes *AB* and AB_2:

$$A + B \underset{k-1}{\overset{k1}{\rightleftharpoons}} AB \tag{7}$$

$$AB + B \underset{k-2}{\overset{k2}{\rightleftharpoons}} AB_2 \tag{8}$$

Thus, a system of non-linear differential equations describe the instantaneous rates for the formation of *B, AB,* and AB_2:

$$\frac{d[B]}{dt} = -k_1[A][B] + k_{-1}[AB] - k_2[AB][B] + k_{-2}[AB_2] \tag{9}$$

$$\frac{d[AB]}{dt} = k_1[A][B] - k_{-1}[AB] - k_2[AB][B] + k_{-2}[AB_2] \tag{10}$$

$$\frac{d[AB_2]}{dt} = k_2[AB][B] - k_{-2}[AB_2] \tag{11}$$

Modeling the rate of formation of *B* from *AB* using Eq. 2 for monovalent binding (Fab) and from AB_2 using Eqs. 9-11 for bivalent binding (IgG) by numerical analysis demonstrates the slow apparent dissociation rate that arises from perfectly efficient cross-linking (Fig. 2 and Table 1).

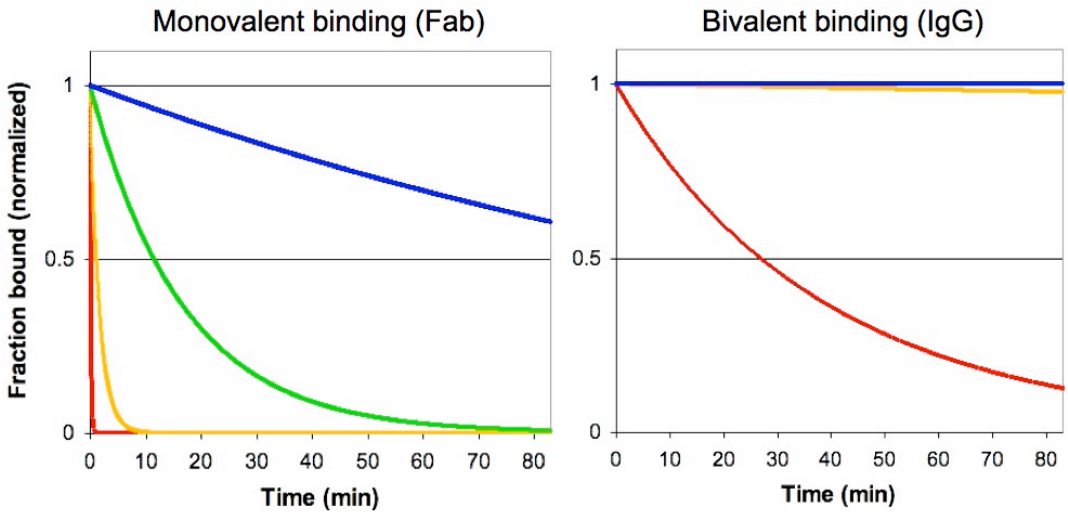

Figure 2. Modeling the dissociation to *B* from *AB* (Fab) and AB_2 (IgG). In both panels, dissociation phases are calculated for 85 minutes. Intrinsic association rates were fixed at 10^5 $M^{-1}s^{-1}$ and models were generated using a range of values for intrinsic dissociation rates of 10^{-1} s^{-1} to 10^{-4} s^{-1}, yielding intrinsic equilibrium dissociation constants of 1 µM (●), 100 nM (●), 10 nM (●), and 1 nM (●). Simulated curves of bivalent binding with intrinsic affinities of 100 nM, 10 nM, and 1 nM were nearly identical such that the curves appear indistinguishable.

Table 1. Half-life values ($t_{1/2}$) of antibody-antigen complexes calculated from models presented in Fig. 2. Values for dissociation involving a monovalent interaction (Fab) were calculated using the equation $t_{1/2} = \ln(2)/(60k_{-1})$. Half-life values for dissociation involving a bivalent interaction (IgG) were derived by inspection or by approximation using the equation for first-order exponential decay.

		$t_{1/2}$ (min)	
k_{-1} (s^{-1})	k_D (nM)	Fab	IgG
10^{-1}	1000 nM	0.12	27
10^{-2}	100 nM	1.2	~3,000
10^{-3}	10 nM	12	~200,000
10^{-4}	1 nM	120	> 200,000

The importance of avidity to virus neutralization was elegantly demonstrated in a study of poliovirus, a non-enveloped icosahedral virus containing 30 two-fold symmetric axes. The authors were able to demonstrate that antibody binding saturates near the expected value of 30 bivalent antibodies per virus particle and that cleaving the antibodies such that the Fab arms became unlinked led to a substantial increase in the molar concentration required to inhibit infection (16). Thus, the bivalent nature of IgG antibodies facilitates binding to and neutralization of viruses.

Evidence for avidity enhancement in the neutralization of enveloped viruses

In the absence of bivalent binding (*i.e.*, cross-linking) or confounding factors such as an increase in the potency of an IgG relative to one of its component Fabs arising simply from its larger size, the maximum difference in neutralization potency between these architectures should be two-fold for the reasons stated previously. Thus, the direct comparison of neutralization potencies for Fabs and IgGs against different viruses can be used as a semi-quantitative assay for cross-linking efficiency.

If cross-linking is necessary for antibody-mediated neutralization at concentrations that are therapeutically relevant, then it should be possible to isolate antibodies that exhibit efficient cross-linking from individuals that have successfully cleared pathogens or been effectively vaccinated against them. Vaccines have been developed for hepatitis B, measles, and influenza type A, all of which are enveloped viruses like HIV. In addition, passively administered antibody therapies exist for both hepatitis B and respiratory syncytial virus (RSV) – another enveloped virus. In stark contrast to what has been observed for HIV, comparisons of IgG antibodies and their Fab fragments reactive to RSV

and influenza type A have demonstrated molar differences in neutralization that are in excess of 1000-fold (Fig. 3). The demonstration that some of these viruses are permissive to highly efficient cross-linking is indicative of the possibility that such viruses share structural features absent from HIV.

Given that avidity primarily derives its effect by limiting the rate of dissociation, a prediction for the difference in potency between an IgG and a Fab as a function of k_{-1} would be that as the value for k_{-1} decreases so should the difference in potencies between the two architectures. For example, one group of researchers created a library of mutants of the antibody Palivizumab, which neutralizes RSV and is used as a prophylaxis (15). Consistent with this prediction, the authors found that as they decreased the intrinsic k_{-1}, thereby increasing the neutralization potency of the Fab, the neutralization potency of the IgG remained relatively unchanged (15) (Fig. 4). In this sense, *one may think of avidity as acting as a buffer to de-optimization of the antibody-antigen interface* (*e.g.,* a pathogen that evades antibody binding by mutation), further underscoring the role that avidity could be playing in antibody-mediated neutralization.

In asking the question of how the topology of spikes might differ between HIV and other enveloped viruses in such a way as to make them more permissive to efficient cross-linking by antibodies, it is helpful to examine the available data from studies by electron microscopy. Cryo-preserved virus samples can be imaged at low-nanometer resolutions such that individual proteins may be resolved on the surfaces of the viruses and reconstructed in three-dimensional space by tomography. Tomographic reconstructions of whole HIV particles have only recently become available (17-19), but they are consistent with older biochemical data that showed a relatively low abundance of spikes on the viral surface (20).

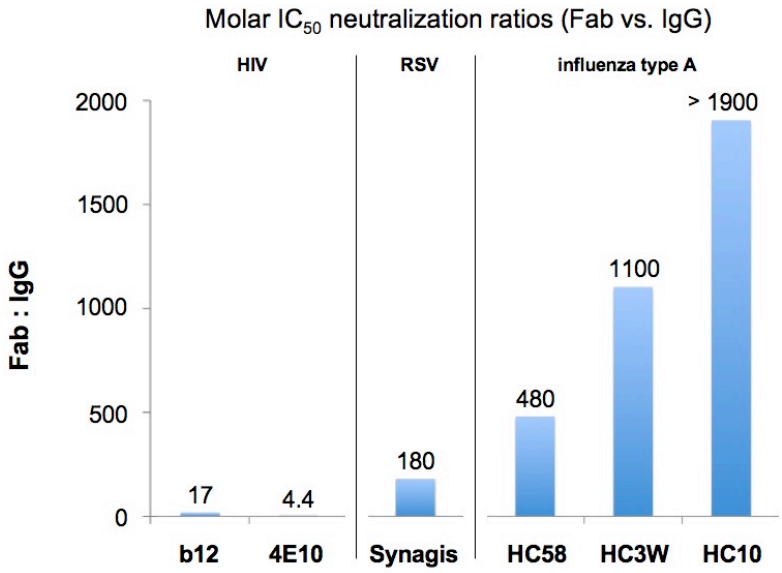

Figure 3. Comparison of IC_{50} neutralization values reported for antibodies as Fabs and intact IgGs (ratios for respiratory syncytial virus (RSV) were calculated from Fab/IgG IC_{50} values reported in (15); ratios for influenza type A (IA) were calculated from Fab/IgG IC_{90} values reported in (21) assuming a Hill coefficient of 1).

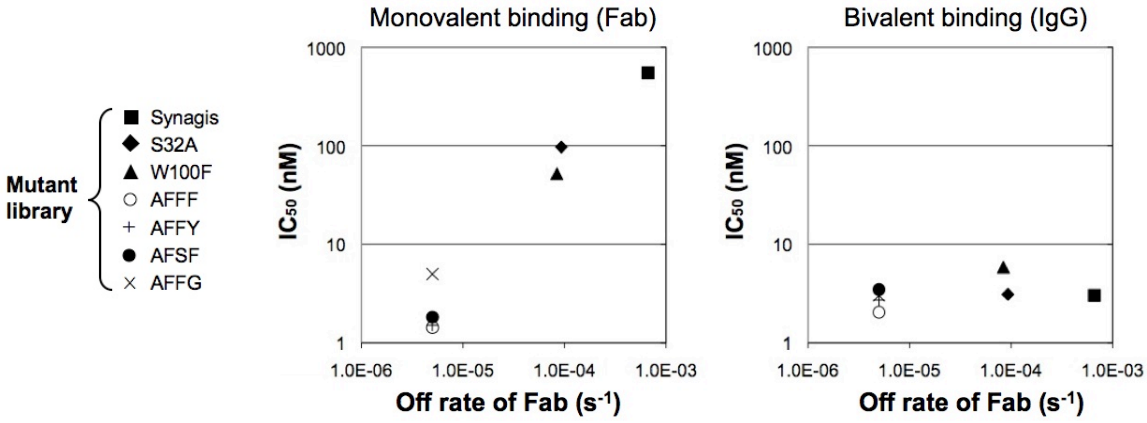

Figure 4. Comparison of neutralization potencies for Palivizumab and affinity-improved mutants with slower intrinsic dissociation constants (reported in (15)). IC_{50} values were reported for the antibodies as Fabs and as intact IgGs.

The Island Effect

Enveloped viruses contain a cell-derived membrane in which viral antigens are acquired during budding from the host cell. An examination of electron micrographs of enveloped viruses for which antibody-mediated neutralization is known to be critical to the control and/or elimination of infection (22-24) reveals a high density of viral spikes on the surfaces of these viruses (Fig. 5). For example, influenza type A virus contains ~450 spikes, which are spaced at intervals ≤ 10 nm (Fig. 5*B*). Similarly, the spikes on measles and hepatitis B virus are closely spaced (Fig. 5*A* and 5*C*). However, biochemical studies and three-dimensional electron microscopic reconstructions revealed that HIV appears to have only 14 ± 7 spikes per virus particle (17, 18, 20, 25) (Fig. 5*D*), probably arising tandem endocytosis motifs that limit the concentration of spikes on the cell surface and the labile nature of the non-covalent gp120-gp41 complex (26, 27).

An analysis of nearest neighbor distances between individual spikes on HIV particles revealed that most of the spikes are separated by distances that far exceed the 12-15 nm reach of the two Fab arms of an IgG (Fig. 5*E*) (17). Given evidence of interactions between gp41 and the viral matrix protein of HIV (28, 29) as well as restricted spike mobility and the inability to cross-link epitopes within a spike (see Chapter 2), these large inter-spike separations may represent an insurmountable barrier to efficient cross-linking by naturally produced anti-HIV antibodies. This model predicts that the only exceptions to the poor efficacy of a monoclonal anti-HIV antibody should be for the condition where the intrinsic affinity of the Fab for a particular strain of HIV is strong enough to be comparable to the avidity-enhanced affinity that would be observed under conditions of efficient cross-linking.

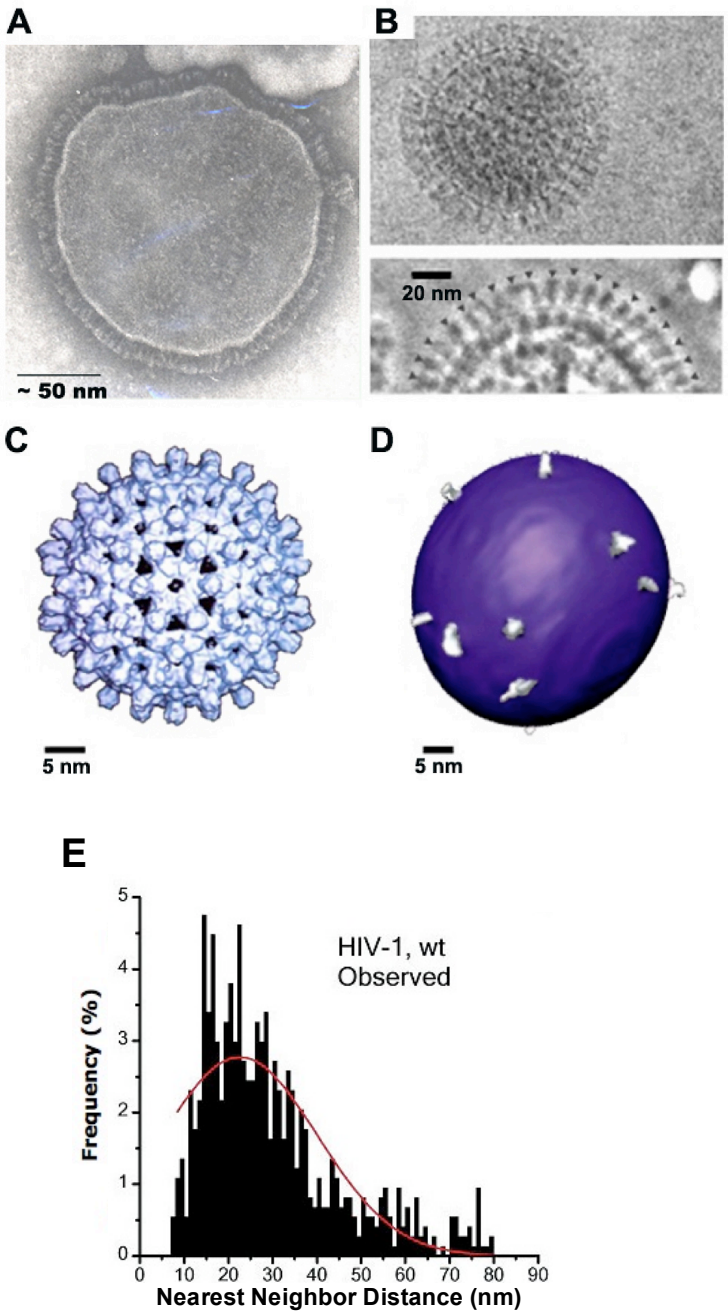

Figure 5. Available structures of enveloped viruses showing spike densities derived by electron microscopy. (*A*) Measles virus (adapted from (30)). (*B*) Influenza type A. Black triangles denote individual spikes in the lower panel (adapted from (31)). (*C*) Hepatitis B virus (adapted from (32)). (*D*) HIV (adapted from (17)). (*E*) Bar graph of the distribution of nearest neighbor distances between HIV envelope spikes (adapted from (17)).

An exception to the island effect: anti-carbohydrate antibodies

Approximately 25 N-linked glycosylation sites are conserved on gp120 (33), although the locations of the sites may vary between strains, such that approximately half of its molecular weight is composed of carbohydrate (34). This feature likely presents anti-carbohydrate antibodies an opportunity to cross-link antigen within a single viral spike. Although antibodies that recognize viral carbohydrates are rare because they are made by host enzymes and therefore expected to be non-immunogenic, one potent bNAb against HIV, 2G12, does recognize a constellation of viral carbohydrates within a single gp120 subunit (35). This unexpected antigenicity is probably related to the mannose content arising from inefficient processing of sterically occluded high-mannose N-linked glycans (36).

Carbohydrate recognition by 2G12 is accomplished using an unusual domain-swapped structure in which the two Fabs create a single antigen recognition region with two rigidly arranged binding sites separated by ~3.5 nm (37). We recently isolated and characterized a naturally occurring dimeric form of 2G12 containing four Fabs instead of two, and the dimeric form exhibited ~50-fold increased neutralization potency across a range of clade B HIV strains compared to monomeric 2G12 (Appendix F). Although it has been shown that gp120 can easily mutate to change its carbohydrate topology (33), which may explain why 2G12 does not show broad cross-reactivity across known strains of HIV (38), the apparent ability of 2G12 to efficiently cross-link antigen makes anti-carbohydrate antibodies with specificities similar to 2G12 a potential source of potent (though perhaps clade-specific) antibodies.

Circumventing the island effect

If the island effect hypothesis is correct, it predicts that attempts to raise NAbs against HIV by injection of purified antigens or attenuated or killed viruses are predestined to fail because too few of the elicited antibodies will bind with high enough intrinsic affinities to the virus to be of practical use. Even if such antibodies were elicited, exposure to strains of HIV whose relevant epitopes do not adequately match those of the strain used for vaccination, a likely scenario, are likely to substantially limit their prophylactic value because they will lack the buffering effect of avidity against natural variation. However, novel antibody architectures may provide a path to negating the island effect, as it may be possible to construct a bivalent antibody in which both of its Fabs are capable of simultaneously binding to epitopes within a single virus spike, eliminating the challenge of accommodating the wide range of nearest neighbor distances between spikes.

The following results summarize ongoing efforts to develop such architectures. Thus far, two different strategies have been examined as candidates for a new hinge extension technology: random coil extension (RCE), and protein fusion extension (PFE). The RCEs were encoded using the $(Gly_4Ser)_x$ sequence (39). Candidates for the PFEs were derived using well-characterized proteins for which high resolution X-ray crystal structures exist, showing that they adopt extended conformations – such candidate proteins included CD4 (40), invasin and a truncation thereof (41), a sequence composed of immunoglobulin domains 168-170 from titin (42), and a tandem repeat of two fibronectin type III domains from neogenin (Yang F, Björkman PJ, unpublished results) (Fig. 6).

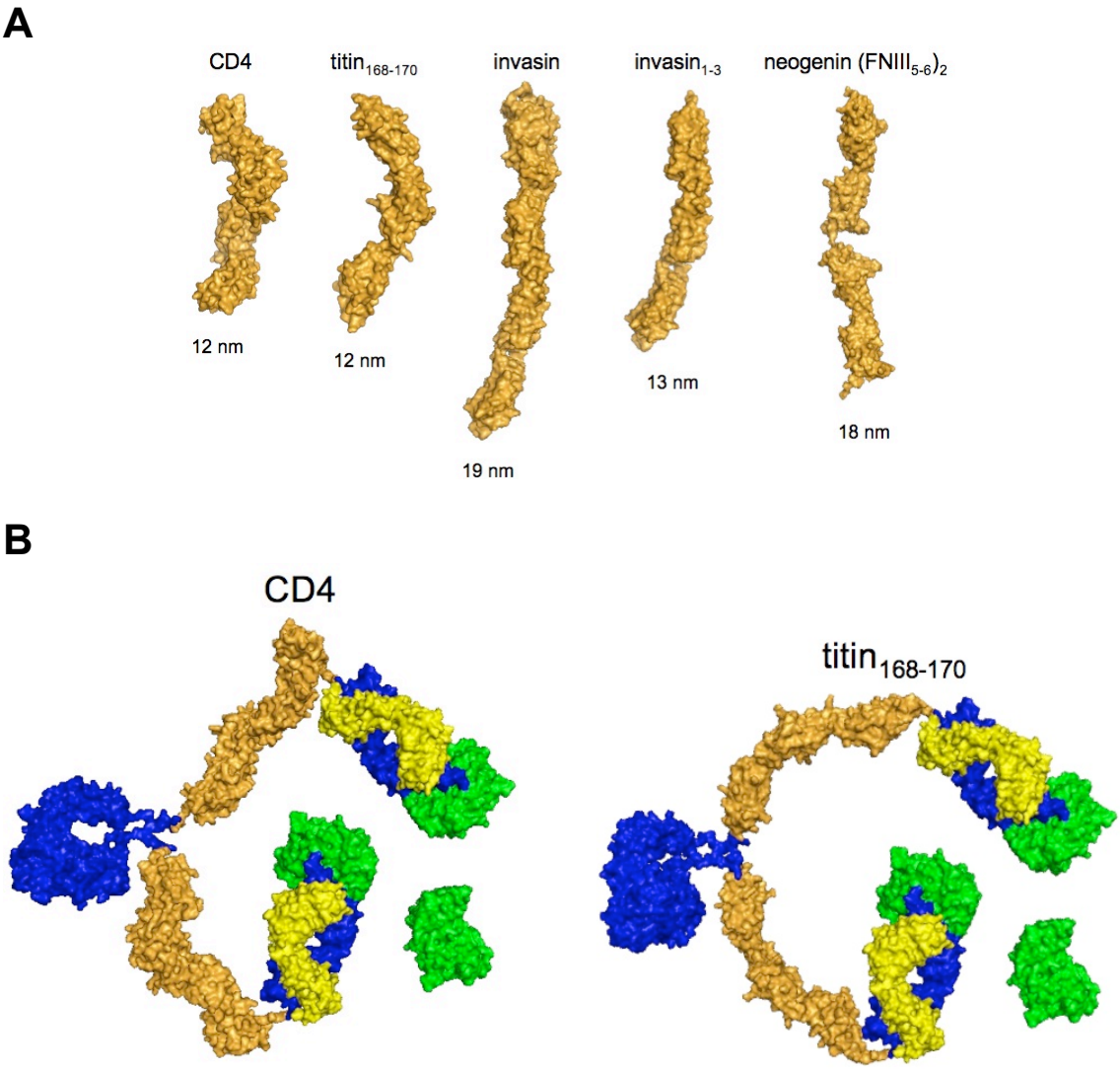

Figure 6. Protein fusion linker candidates and models. (*A*) Candidates for protein fusion linkers differing in length and flexibility (*i.e.*, the hinge domain of CD4 or the two identical neogenin fragments linked by a GlySer sequence versus the relatively rigid structure of invasin and a truncated form, invasin$_{1\text{-}3}$). (*B*) These top view models are examples of protein fusion extensions (PFE) and are based on the trimeric spike model presented in Chapter 2 using the coordinates from high-resolution X-ray crystal structures of gp120 docked to available tomographic reconstructions of intact spikes on cryo-preserved virus particles (gp120, green; PFE, gold; Fab, blue and yellow; Fc, blue).

Results

Characterization of IgGs with RCEs

IgG forms of b12, 2G12, 4E10, and 2F5 were expressed with RCEs 1, 3, 5, and 7 repeats of a Gly_4Ser sequence inserted into the hinge region separating the CH_1 domain from the CH_2 domain in an IgG1 architecture N-terminal to the naturally occurring DKTHT hinge sequence. All proteins were purified by Protein A affinity chromatography followed by SEC. When analyzed by reduced SDS PAGE, slight increases in the molecular weights of the heavy chains with increasing hinge length were observed (Fig. 7*B*).

Protein expression decreased as a function of increased linker length for constructs with 1, 3, and 5 Gly_4Ser repeats, and little to no expression was observed for constructs with 7 repeats for some IgGs (Table 2). This sharp decline in expression was observed for all antibodies tested, suggesting that RCEs of this length introduce a general limit to the folding of IgG sequences or might inhibit dimerization either between the heavy chains or between the heavy chains and light chains. In addition, reduced amounts of 2G12 dimer were recovered from the RCE expressions with more than one Gly_4Ser insertion, indicating that extended hinge sequences prevent the intermolecular domain swapping observed for the wild type architecture of this antibody (Appendix F). Although the sequences were codon optimized, more recent advances in codon optimization algorithms may provide an opportunity to offset the losses in protein yield (43, 44).

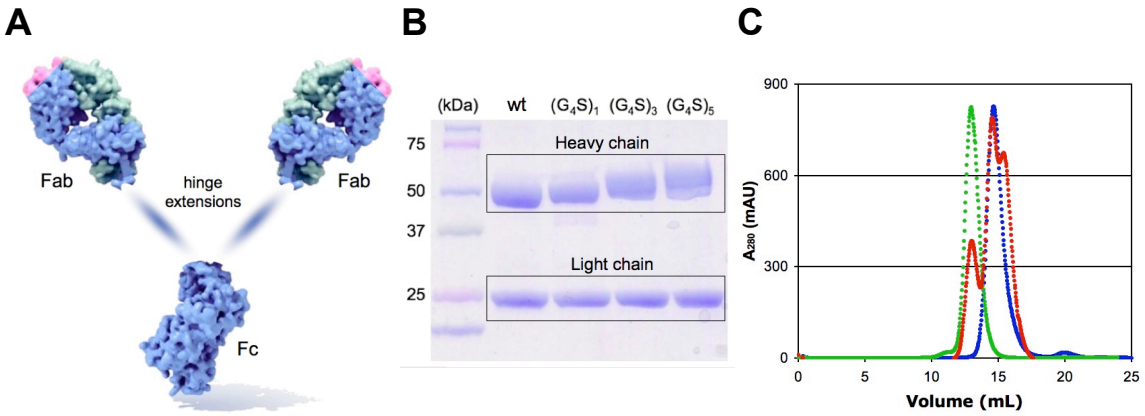

Figure 7. (*A*) Schematic of the structure of a human IgG antibody of subclass 1 with RCEs. Pink coloring denotes the locations of antigen recognition sites (adapted from U.S. National Library of Medicine). (*B*) Reduced SDS PAGE results for IgG b12 with Gly_4Ser RCEs of increasing length. (*C*) Gel filtration profile of Fab 2G12 (blue), IgG 2G12 $(G_4S)_1$ after purification (green) and after one month of storage in TBS at 4 °C (red).

Table 2. Protein yields for 1 L expressions of each of the RCE constructs.

	Total yield (mg/L) and percentage of wild type yield				
Antibody	**wt**	**$(Gly_4Ser)_1$**	**$(Gly_4Ser)_3$**	**$(Gly_4Ser)_5$**	**$(Gly_4Ser)_7$**
b12	6	6 (100%)	6 (100%)	5 (83%)	0.5 (8%)
2G12	20	15 (75%)	5 (25%)	4 (20%)	2 (10%)
4E10	7	4 (57%)	3 (43%)	2 (28%)	0
2F5	4	2 (50%)	1.5 (38%)	1 (25%)	0

It was also observed that precipitation or degradation into Fab and Fc fragments occurred following storage for periods of > 1 month at 4 °C in TBS (Fig. 7*C*), yet neither the IgGs nor the scFvs described in Chapter 2 exhibited degradation after storage for similar lengths of time. Interestingly, these effects were not observed for several of the $(Gly_4Ser)_5$ RCEs that had been stored as Protein A eluates (a citrate buffer neutralized with Tris) and purified by SEC in TBS only after long-term storage. Thus, it might be possible to inhibit the apparent instability of RCEs with alternative buffer conditions.

In theory, the ability of an IgG to bind with avidity will be reduced as the hinge length increases because it reduces the effective concentration of the Fab arms (45). To examine whether the RCE antibodies exhibited this predicted effect, wild type IgG, RCEs with the $(Gly_4Ser)_5$ extension (the longest one that expressed efficiently) and monomeric Fab forms were injected over a CM5 surface displaying 500 RU of either monomeric gp120 or gp41. Half-life times ($t_{1/2}$) were then calculated from their apparent dissociation rate constants by approximation with a model for first-order exponential decay (Fig. 8 and Table 3). No significant differences in $t_{1/2}$ values were observed between the wild type and RCE antibodies, demonstrating that the ability to bind with avidity remained intact. As expected, the $t_{1/2}$ values for all of the Fabs were significantly faster with the exception of 2G12. The similar rate of dissociation for the 2G12 Fab as compared to the bivalent constructs is likely due to the domain swapped structure remaining intact.

To examine whether RCEs exhibited an avidity enhancement during neutralization, which would be reflected as a decrease in the IC_{50} values relative to the wild type IgG, the potency of each of the antibodies were compared in an *in vitro*

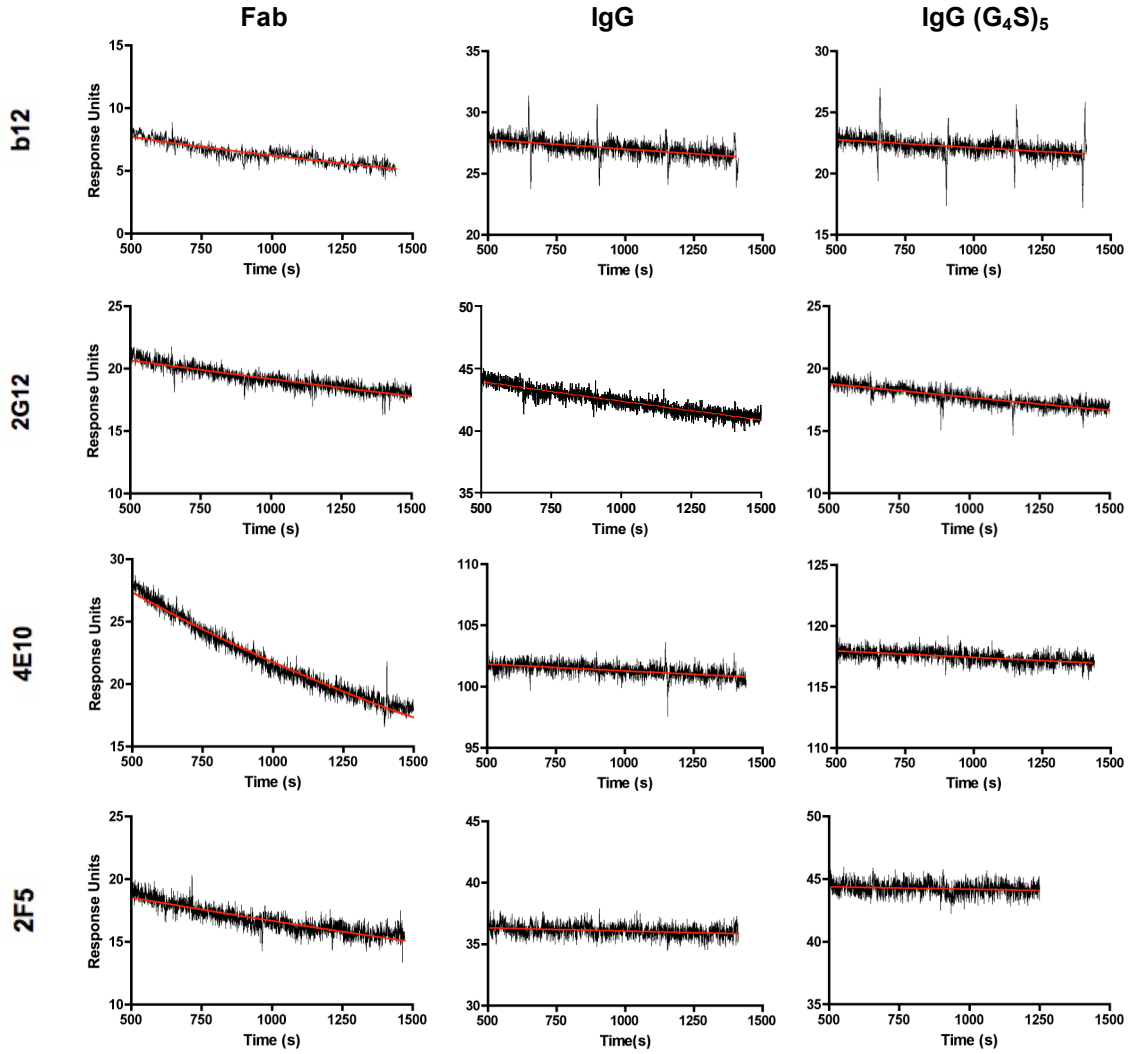

Figure 8. SPR dissociation curves for Fab, IgG, and IgG $(G_4S)_5$ constructs bound to immobilized monomeric gp120 (b12 and 2G12) or immobilized gp41 (4E10 and 2F5).

Table 3. Half-life times ($t_{1/2}$) calculated from dissociation curves in Fig. 8.

	$t_{1/2}$ (min)		
Antibody	**Fab**	**IgG wt**	**IgG $(G_4S)_5$**
b12	28	200	200
2G12	77	160	96
4E10	25	1000	1300
2F5	55	800	1300

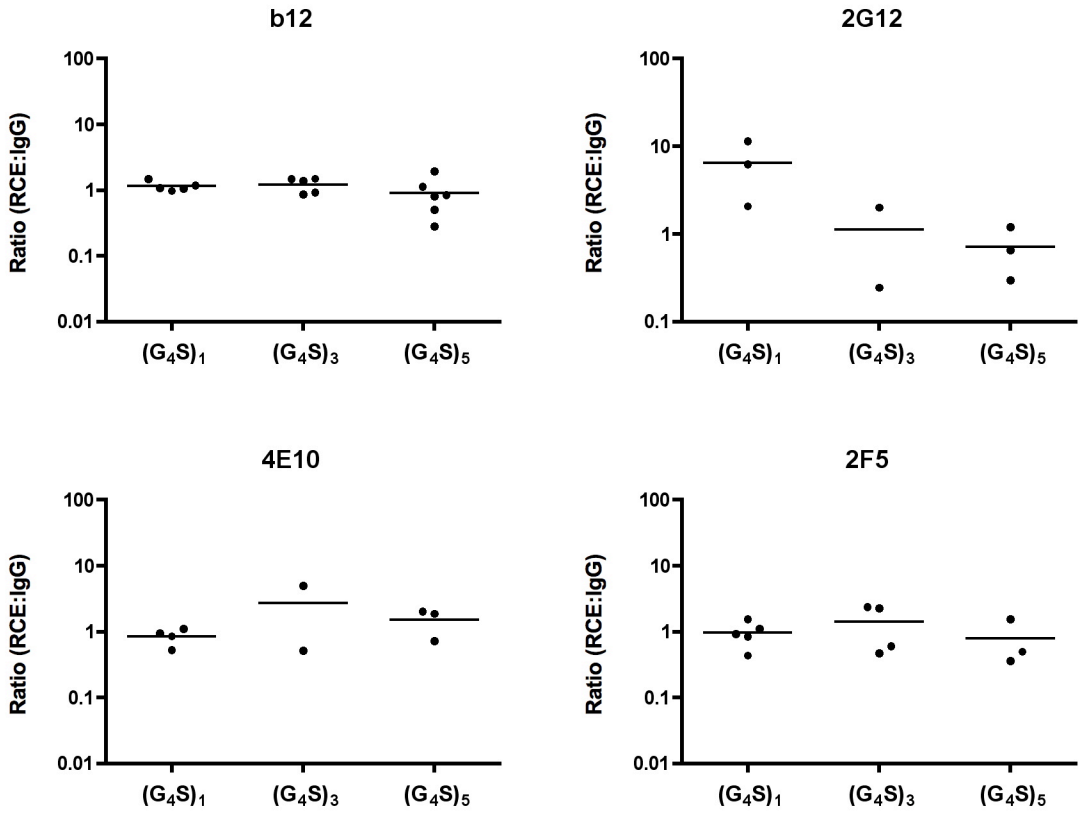

Figure 9. Results of the *in vitro* neutralization assay comparing wild type IgG constructs with RCEs. Values were calculated as the ratio of the molar IC_{50} determined for the RCE divided by the molar IC_{50} determined for the parental IgG. The IgG 2G12 $(Gly_4Ser)_3$ construct was non-neutralizing for strain QH0692.42.

neutralization assay. Each of the antibody constructs was tested against virus strains from clade B (Fig. 9).

When comparing the molar IC_{50} values for the RCEs with the values determined for the wild type IgGs, nearly all were within a few fold of each other. One significant exception was observed for 2G12 versus strain QH0692.42. Whereas wild type IgG 2G12 neutralized this strain with an IC_{50} of 59 nM, the 2G12 RCE with a single Gly_4Ser repeat was 6-fold less potent (IC_{50} value of 360 nM) and the RCE with three Gly_4Ser repeats was completely non-neutralizing. It was also observed that Fab 2G12 is also non-neutralizing against this strain.

Characterization of IgGs with PFEs

Expression tests were completed for all of the protein fusion extensions (PFEs). Each construct was purified by protein A affinity chromatography followed by SEC. While some of the 4E10 and 2G12 PFEs and one for 2F5 yielded between 0.5 and 1 mg/L (Figs. 10 and 11), none of the b12 constructs yielded measurable quantities of purified protein. The b12 constructs were of most interest because it was the Fab b12 structure bound to the trimeric spike that was used for the rational design of the PFEs (Fig. 6*B*). This indicates that for future studies it may be necessary to start with simpler designs that express well and then build on those. Thus, a set of small single domain candidates to serve as protein fusions are currently in development, which, provided they express well, will be used in multi-domain PFEs, each separated by short flexible linkers.

The PFEs that did express were evaluated for their abilities to bind immobilized antigen by SPR and for their abilities to neutralize HIV *in vitro* (Fig. 12 and Table 4). For

both 4E10 and 2F5, the PFEs that did express at levels sufficient to test (invasin and invasin$_{1-3}$ for 4E10 and invasin$_{1-3}$ for 2F5), sensograms for binding to immobilized gp41 were comparable to their respective wild type IgGs (Table 4). However, whereas the kinetics for dissociation of IgG 2G12 with an invasin$_{1-3}$ PFE were observed to be comparable relative to wild type IgG, the rate of dissociation for the 2G12 neogenin PFE was observed to be significantly slower ($t_{1/2}$ of 1200 min versus 160 min, Tables 3 and 4). Interestingly, dimeric IgG 2G12, which was also examined by SPR (Fig. 12 and Table 3), showed a slightly faster rate of dissociation than its monomeric form ($t_{1/2}$ of 65 min). Thus, in spite of its ~50-fold greater potency in neutralization (Appendix F), there appears to be no evidence of an avidity enhancement for dimeric IgG 2G12 when binding monomeric gp120 immobilized on a CM5 surface, suggesting that the enhanced potency of dimeric 2G12 derives from an ability to bind glycans on multiple gp120 monomers.

When examined for their respective abilities to neutralize HIV (strain 6535.3), the PFEs were considerably less potent than their respective wild type IgGs (Fig. 13). These results support the findings presented in Chapter 2 of steric occlusion for the 4E10 epitope in that the short linkage between the Fab and the PFE (-GGSGGSA-) may further inhibit access to its epitope. However, these data represent the first evidence of a similar effect for 2F5, whose epitope is immediately N-terminal to the 4E10 epitope, indicating that the MPER as a whole may be sterically occluded.

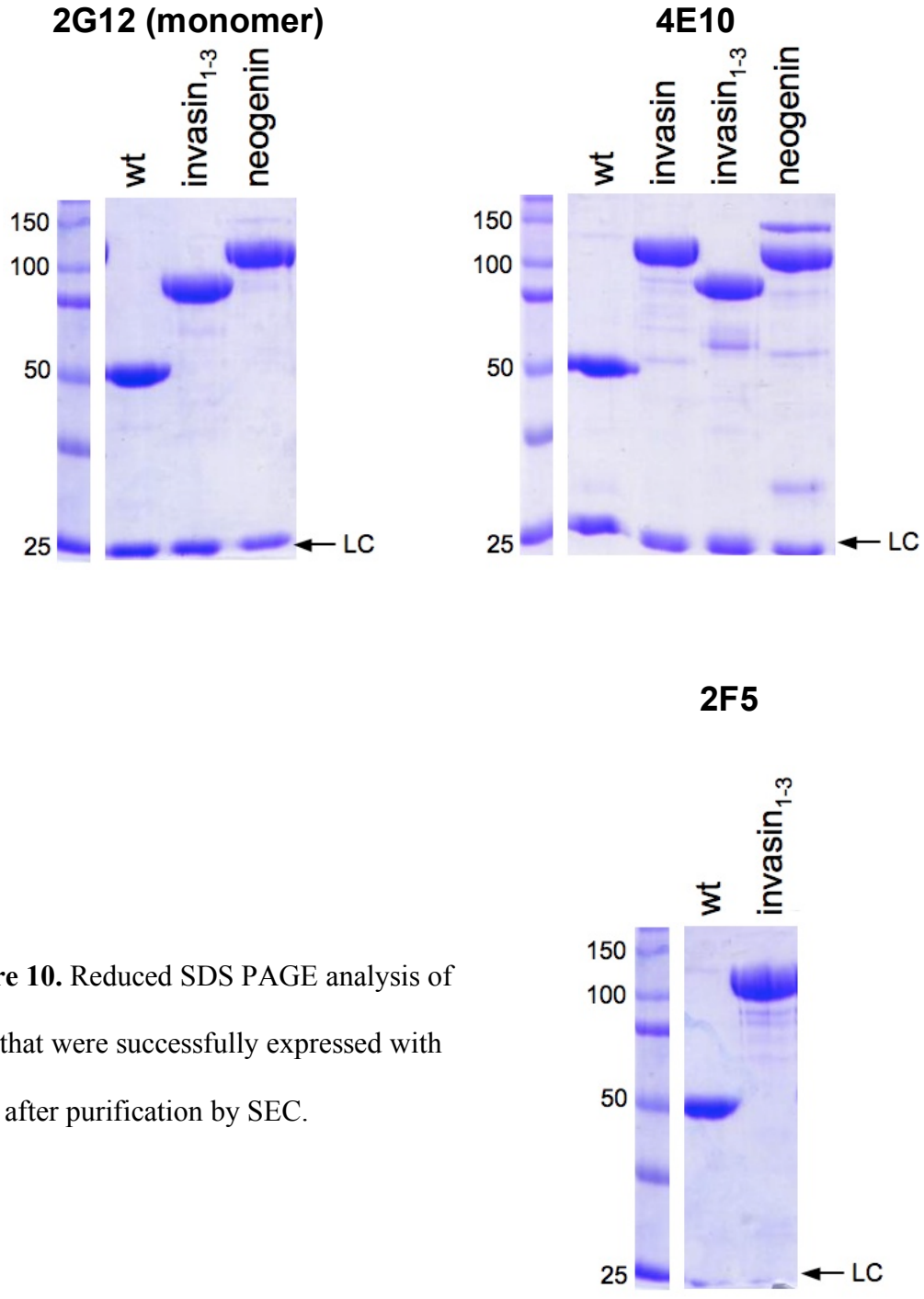

Figure 10. Reduced SDS PAGE analysis of IgGs that were successfully expressed with PFEs after purification by SEC.

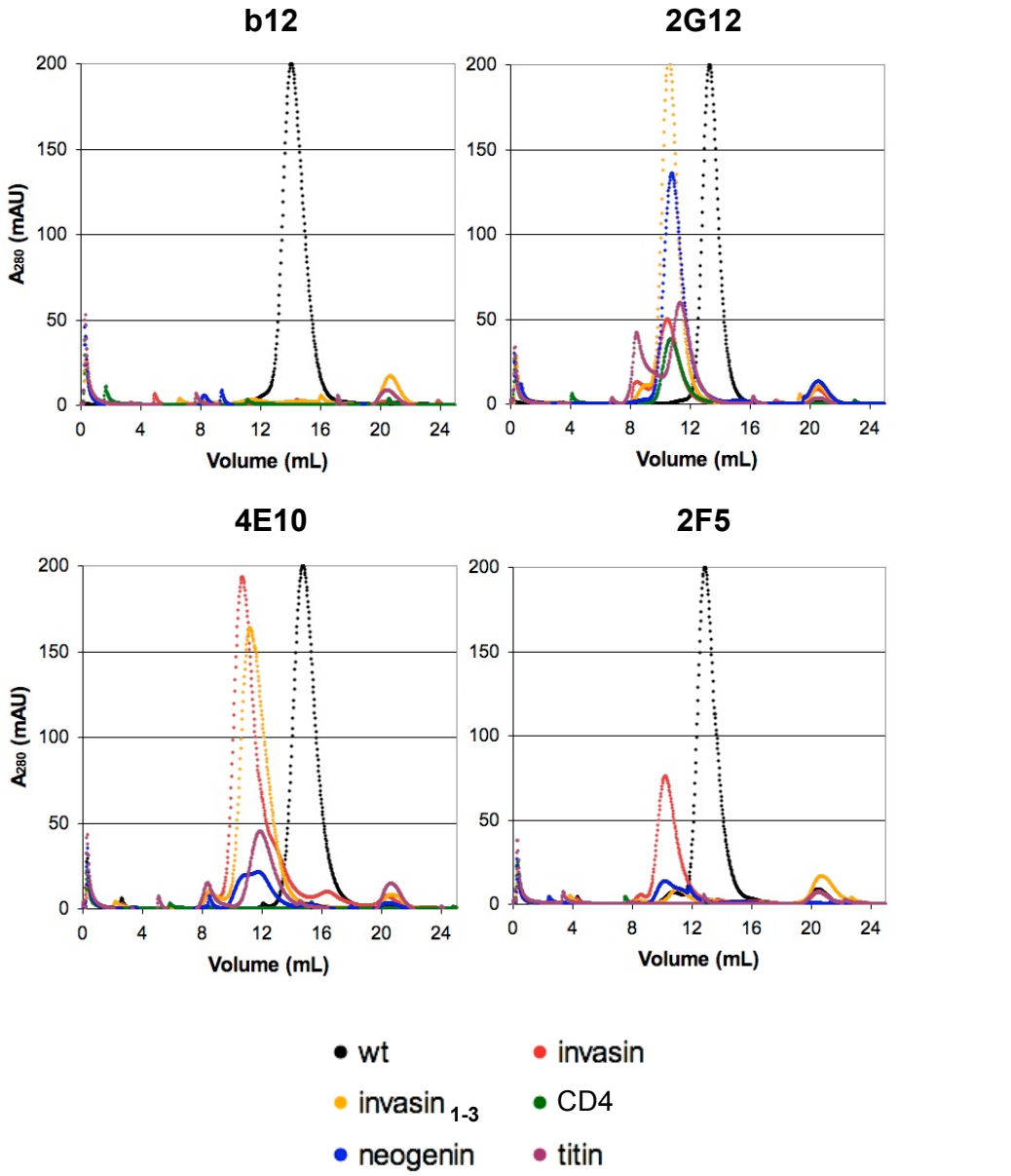

Figure 11. Gel filtrations profiles for IgGs with protein fusion extensions. Chromatograms for wt IgGs were normalized to peak heights of 200 mAU (~1 mg). The chromatograms for the hinge extended IgGs are shown untransformed such that differences in peak heights reflect differences in yield from 1 L of supernatant. The void peak is at 8.5 mL.

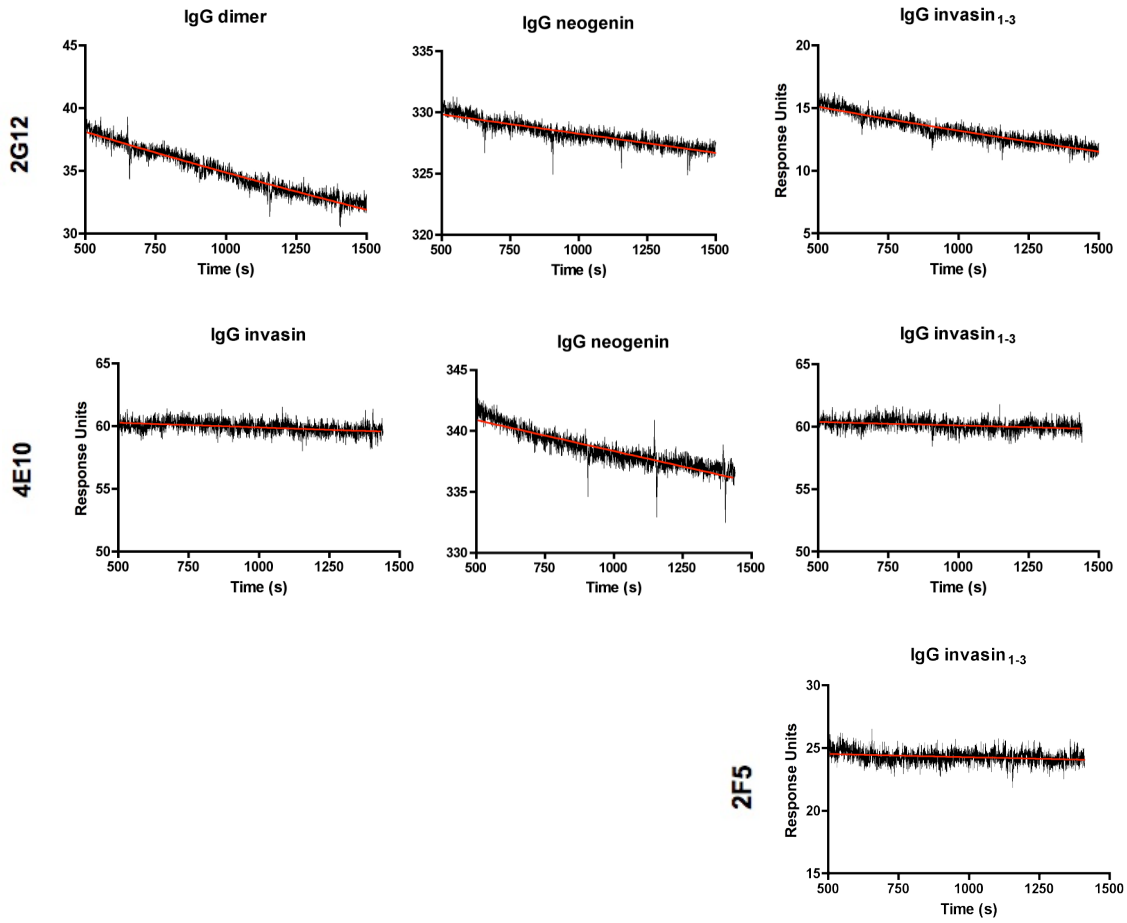

Figure 12. Dissociation curves for PFE constructs and 2G12 dimer bound to immobilized monomeric gp120 (2G12) or immobilized gp41 (4E10 and 2F5).

Table 4. Half-life times ($t_{1/2}$) calculated from the dissociation curves of dimeric IgG 2G12 and PFEs in Fig. 11.

Antibody	$t_{1/2}$ (min)	$t_{1/2}$ wt IgG : $t_{1/2}$ PFE
2G12 dimer	65	2.5
2G12 neogenin	1,200	0.14
2G12 invasin$_{1-3}$	43	3.8
4E10 invasin	920	1.1
4E10 neogenin	770	1.3
4E10 invasin$_{1-3}$	1,200	0.83
2F5 invasin$_{1-3}$	500	1.6

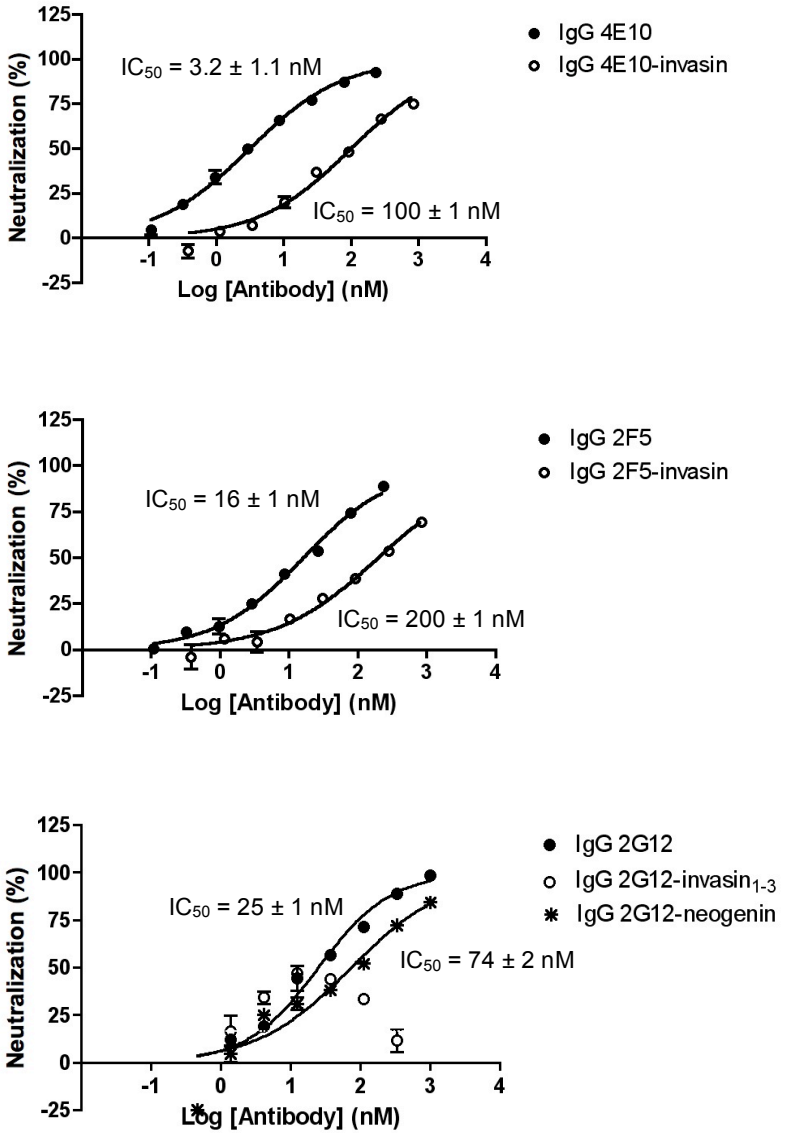

Figure 13. Comparison of neutralization activities for PFEs versus wild type IgGs (HIV strain 6535.3).

With respect to the 2G12 PFEs, no evidence was observed for increased neutralization potency. Given the increased size of the 2G12 PFEs and assuming that the domain swapped architecture of the 2G12 binding site is intact for these constructs, these results support the likelihood that the increased potency of dimeric IgG 2G12 derives from the presence of two adjoining domain swapped Fab dimers rather than the alternative possibility that the presence of two Fc domains increases its ability to sterically block the virus from binding to target cells. Thus, the reason for the lack of neutralization potency for purified 2G12 Fab and the precise mechanism by which this anti-carbohydrate antibody blocks infection remains unresolved.

The behavior of 2G12 with a tandem neogenin PFE was unexpected in that it could neutralize the virus at low concentrations with similar if not better potency as compared to monomeric IgG 2G12 (Fig. 13). However, above concentrations of ~20 nM, neutralization rapidly decreased to zero. Repeating this experiment yielded exactly the same result (data not shown). Additionally, injections of this construct over immobilized monomeric gp120 indicated an unexpectedly high maximum response (R_{max}) relative to monomeric IgG 2G12 that cannot be accounted for by its increased molecular weight ($R_{max} = C_{ligand} * S * MW_{analyte} / MW_{ligand}$ where R_{max} is the maximum response, C_{ligand} is the amount of immobilized ligand, and S is the stoichiometry of the interaction) (Fig. 12). Moreover, the calculated half-life for binding was ~7-fold slower than monomeric IgG 2G12 (1,200 min versus 160 min, Tables 3 and 4). A possible explanation for this behavior would be the presence of some affinity between neogenin and the 2G12 combining site such that as the neogenin PFE bound to gp120 on the chip surface, more binding sites were introduced, thereby permitting increased binding. Likewise, high concentrations in the neutralization

assay would enable the construct to act as a competitive inhibitor, rationalizing the drop in neutralization potency with increasing concentration of the inhibitor.

Discussion

The neutralization data for the RCEs indicate that extending the hinge region of an IgG using unstructured Gly_4Ser repeats does not enhance neutralization potency despite the observation in the binding analysis that the potential for avidity remains intact for all hinge extension lengths tested. There are at least three possible explanations for this observation:

(i) despite the low density of spikes on the surface of HIV, spikes can diffuse throughout the lipid bilayer at a rate that is not limiting to bivalent binding regardless of the distance between antibody combining sites;

(ii) the spikes are diffusion limited but the assumption that an unstructured linker enables the Fabs to efficiently sample extended conformations is false;

(iii) the spikes are diffusion limited and all spikes must be bound for neutralization to occur, but the set of nearest neighbor distances that describes the distribution of spikes for most virions leaves a significant portion of the spikes outside the reach of the antibodies with RCEs examined here.

The first explanation is not supported by the current results in which it was shown that a scBvFv architecture that has a maximum distance between the two combining sites of 11 nm is less potent than an IgG architecture where the maximum distance between

combining sites is approximately 15 nm (Chapter 2). For example, in the case of 4E10 it was observed that a scBvFv was equally potent to a monomeric single chain Fv, indicating a complete absence of cross-linking for the scBvFv even though evidence was observed of cross-linking for the IgG. Similarly, increased neutralization potency was observed for IgG b12 over the scBvFv architecture. Together, these data suggest that the distance between combining sites does influence neutralization potency and, consequently, the spikes on the surface of HIV are diffusion limited relative to the kinetics of bivalent binding.

An answer to the second explanation may be derived from a recent paper that compared the fluorescence resonance energy transfer (FRET) efficiency between GFP and YFP as a function of the number of repeats of a $(Gly_2Ser)_2$ linker connecting them (46). Here it was shown that the decrease in FRET efficiency as the linker length increased was consistent with a distribution function that shows a marked broadening in the range of distances sampled and that as each additional repeat of 6 amino acids was inserted, the average distance sampled increased by a decreasing fraction of the ~2 nm that 6 additional residues could theoretically span if fully extended. Consequently, rather than adding 15 nm, the $(Gly_4Ser)_5$ linker of the bivalent IgG (similar in length to CLY9 construct examined in the FRET investigation) probably added on average 4 to 5 nm to the 15 nm reach of the IgGs. An inability of the unstructured Gly_4Ser linkers used in this study to allow the Fabs to efficiently sample extended conformations could explain the lack of increased potency as a function of the number of linker repeats inserted into the hinge region.

The third explanation gives consideration to the stoichiometric requirements for neutralization and the nearest neighbor distribution reported for a set of 40 virions analyzed by electron microscopy (17). In a recent paper, researchers observed that influenza requires 8 to 9 functional spikes to mediate viral entry into a target cell but HIV and two other retroviruses tested required only a single functional spike to mediate successful entry (47). If this model is correct, then all or nearly all spikes must be bound for a single virus particle to be effectively neutralized if one assumes a high number of interactions between the virus particle and a target cell over the course of its lifetime. A counter to this argument was presented in another report in which HIV particles that appeared to be bound to target cells all exhibited what the researchers termed an "entry claw", in which ~5 spikes were involved in coordinating attachment (18). While this does not disprove the one-spike fusion hypothesis, it suggests that multiple spikes with intact CD4 and/or co-receptor binding sites (but not necessarily fusion-competent) are required to create a stable attachment prior to the fusion that may be catalyzed by a single spike.

Given the indications that (*i*) all or nearly all spikes must be bound either to prevent fusion or prevent a stable attachment, (*ii)* spikes are diffusion limited, (*iii*) RCEs are ineffective for expanding the reach of an IgG in this setting, and (*iv*) many HIV spike pairs are separated by distances that make them unrealistic targets for cross-linking, the design of an IgG capable of intra-spike cross-linking probably represents a more tractable goal. Because the distance between identical binding sites on a single spike is probably static, the effectiveness of this architecture would not be limited by potentially confounding factors such as spike mobility and nearest neighbor distribution.

If one considers how evolution appears to have selected for molecules with extended conformations, the linear arrangement of immunoglobulin (Ig) domains (*e.g.,* CD4, VEGF, PDGF) and fibronectin type III (FnIII) domains (*e.g.,* cell adhesion molecules) appear to be common themes compared to the evolution of unstructured linkers (*e.g.,* CD8). For example, a recent crystal structure of domains 168-170 from titin composed of two Ig domains and one FnIII domain revealed an extended conformation of ~12 nm (42), sufficient for the length requirement of b12. Unfortunately, measurable quantities of protein were not isolated for PFEs involving b12, the structure that was used to model and design the hinge extensions. Clearly, alternative approaches to developing structured linkers are required. Other approaches that may prove worthwhile include covalent modifications to couple Fabs *in vitro* using DNA molecules of different lengths or less complex PFEs such as small single domain proteins that are known for high yields and excellent stability.

The successful design of antibodies capable of intra-spike cross-linking could represent a significant advance in human health by providing the first realistic option for prophylaxis by gene therapy for HIV, or as in the case of chemical modification, applicability in a therapeutic setting. Moreover, perfection of a hinge extension technology developed to counteract the island effect that may be thwarting HIV neutralization by conventional antibodies might also be applied to other diseases or pathogens in which binding is avidity-limited.

Materials and Methods

Sequences for RCEs and PFEs were codon optimized and generated by DNA

synthesis. In the case of PFEs, a $(Gly_2Ser)_2$ linker was included at the N-terminus and C-terminus. All PFEs (invasin, $invasin_{1-3}$, CD4, $titin_{168-170}$, and a tandem repeat of $neogenin_{5-6}$) were further analyzed for predicted N-linked glycosylation sites that were subsequently removed with conservative Asn→Asp mutations or in a few cases, Ser/Thr→Ala mutations.

Full-length heavy chain (IgG1 subclass) and light chain (κ) genes were initially subcloned separately into pTT5. The RCEs and PFEs were then cloned immediately 5' to the natural IgG1 hinge sequence and 3' to the codon encoding the Cys residue that participates in the disulfide bond with light chain using the restriction sites NgoM IV and Nhe I previously introduced by PCR.

Methods describing expression, purification, binding assays, molecular modeling, and neutralization assays can be found in Chapter 2.

References

1. 2007 AIDS epidemic update : December 2007 (UNAIDS/WHO, November 2007).
2. Hutter G*, et al.* (2009) Long-term control of HIV by CCR5 Delta32/Delta32 stem-cell transplantation. *N Engl J Med* 360:692-698.
3. Bedimo R*, et al.* (2006) Sustained HIV viral suppression following treatment interruption: an observational study. *AIDS Res Hum Retroviruses* 22:40-44.
4. Roberts JD, Bebenek K, & Kunkel TA (1988) The accuracy of reverse transcriptase from HIV-1. *Science* 242:1171-1173.
5. Trkola A*, et al.* (2005) Delay of HIV-1 rebound after cessation of antiretroviral therapy through passive transfer of human neutralizing antibodies. *Nat Med*. 11(6):615-622.
6. Zwick MB*, et al.* (2001) Neutralization synergy of human immunodeficiency virus type 1 primary isolates by cocktails of broadly neutralizing antibodies. *J Virol* 75:12198-12208.
7. Parren PW*, et al.* (2001) Antibody protects macaques against vaginal challenge with a pathogenic R5 simian/human immunodeficiency virus at serum levels giving complete neutralization in vitro. *J Virol* 75:8340-8347.
8. Lobo ED, Hansen RJ, & Balthasar JP (2004) Antibody pharmacokinetics and pharmacodynamics. *J Pharm Sci* 93:2645-2668.
9. Pero JK, Haas EM, & Thompson NL (2006) Size dependence of protein diffusion very close to membrane surfaces: measurement by total internal reflection with fluorescence correlation spectroscopy. *J Phys Chem B* 110:10910-10918.

10. Drake AW, Myszka DG, & Klakamp SL (2004) Characterizing high-affinity antigen/antibody complexes by kinetic- and equilibrium-based methods. *Anal Biochem* 328:35-43.

11. Darbha R*, et al.* (2004) Crystal structure of the broadly cross-reactive HIV-1-neutralizing Fab X5 and fine mapping of its epitope. *Biochemistry* 43:1410-1417.

12. Edwards MJ & Dimmock NJ (2001) A haemagglutinin (HA1)-specific FAb neutralizes influenza A virus by inhibiting fusion activity. *J Gen Virol* 82:1387-1395.

13. Brunel FM*, et al.* (2006) Structure-function analysis of the epitope for 4E10, a broadly neutralizing human immunodeficiency virus type 1 antibody. *J Virol* 80:1680-1687.

14. Martin-Garcia J, Cocklin S, Chaiken IM, & Gonzalez-Scarano F (2005) Interaction with CD4 and antibodies to CD4-induced epitopes of the envelope gp120 from a microglial cell-adapted human immunodeficiency virus type 1 isolate. *J Virol* 79:6703-6713.

15. Wu H*, et al.* (2005) Ultra-potent antibodies against respiratory syncytial virus: effects of binding kinetics and binding valence on viral neutralization. *J Mol Biol* 350:126-144.

16. Icenogle J*, et al.* (1983) Neutralization of poliovirus by a monoclonal antibody: kinetics and stoichiometry. *Virology* 127:412-425.

17. Zhu P*, et al.* (2006) Distribution and three-dimensional structure of AIDS virus envelope spikes. *Nature* 441:847-852.

18. Sougrat R*, et al.* (2007) Electron tomography of the contact between T cells and SIV/HIV-1: implications for viral entry. *PLoS Pathog* 3(5):571-581.

19. Liu J, Bartesaghi A, Borgnia MJ, Sapiro G, & Subramaniam S (2008) Molecular architecture of native HIV-1 gp120 trimers. *Nature* 455:109-113.

20. Chertova E*, et al.* (2002) Envelope glycoprotein incorporation, not shedding of surface envelope glycoprotein (gp120/SU), Is the primary determinant of SU content of purified human immunodeficiency virus type 1 and simian immunodeficiency virus. *J Virol* 76:5315-5325.

21. Schofield DJ, Stephenson JR, & Dimmock NJ (1997) Variations in the neutralizing and haemagglutination-inhibiting activities of five influenza A virus-specific IgGs and their antibody fragments. *J Gen Virol* 78 (Pt 10):2431-2439.

22. Karlsson Hedestam GB*, et al.* (2008) The challenges of eliciting neutralizing antibodies to HIV-1 and to influenza virus. *Nat Rev Microbiol* 6:143-155.

23. Pantaleo G & Koup RA (2004) Correlates of immune protection in HIV-1 infection: what we know, what we don't know, what we should know. *Nat Med* 10:806-810.

24. Plotkin SA (2001) Immunologic correlates of protection induced by vaccination. *Pediatr Infect Dis J* 20:63-75.

25. Liu J, Bartesaghi A, Borgnia MJ, Sapiro G, & Subramaniam S (2008) Molecular architecture of native HIV-1 gp120 trimers. *Nature* 455(7209):109-113.

26. Egan MA, Carruth LM, Rowell JF, Yu X, & Siliciano RF (1996) Human immunodeficiency virus type 1 envelope protein endocytosis mediated by a highly conserved intrinsic internalization signal in the cytoplasmic domain of

gp41 is suppressed in the presence of the Pr55gag precursor protein. *J Virol* 70:6547-6556.

27. Ye L*, et al.* (2004) Surface stability and immunogenicity of the human immunodeficiency virus envelope glycoprotein: role of the cytoplasmic domain. *J Virol* 78:13409-13419.

28. Benjamin J, Ganser-Pornillos BK, Tivol WF, Sundquist WI, & Jensen GJ (2005) Three-dimensional structure of HIV-1 virus-like particles by electron cryotomography. *J Mol Biol* 346:577-588.

29. Yu X, Yuan X, Matsuda Z, Lee TH, & Essex M (1992) The matrix protein of human immunodeficiency virus type 1 is required for incorporation of viral envelope protein into mature virions. *J Virol* 66:4966-4971.

30. Rosenblatt S. http://www.tau.ac.il/lifesci/departments/biotech/members/rozenblatt/figures.html.

31. Conway JF*, et al.* (1997) Visualization of a 4-helix bundle in the hepatitis B virus capsid by cryo-electron microscopy. *Nature* 386:91-94.

32. Yamaguchi M, Danev R, Nishiyama K, Sugawara K, & Nagayama K (2008) Zernike phase contrast electron microscopy of ice-embedded influenza A virus. *J Struct Biol* 162:271-276.

33. Wei X*, et al.* (2003) Antibody neutralization and escape by HIV-1. *Nature* 422:307-312.

34. Poignard P, Saphire EO, Parren PW, & Burton DR (2001) gp120: Biologic aspects of structural features. *Annu Rev Immunol* 19:253-274.

35. Scanlan CN, *et al.* (2002) The broadly neutralizing anti-human immunodeficiency virus type 1 antibody 2G12 recognizes a cluster of alpha1-->2 mannose residues on the outer face of gp120. *J Virol* 76:7306-7321.

36. Lin G, *et al.* (2003) Differential N-linked glycosylation of human immunodeficiency virus and Ebola virus envelope glycoproteins modulates interactions with DC-SIGN and DC-SIGNR. *J Virol* 77:1337-1346.

37. Calarese DA, *et al.* (2003) Antibody domain exchange is an immunological solution to carbohydrate cluster recognition. *Science* 300:2065-2071.

38. Binley JM, *et al.* (2004) Comprehensive cross-clade neutralization analysis of a panel of anti-human immunodeficiency virus type 1 monoclonal antibodies. *J Virol* 78:13232-13252.

39. Bird RE, *et al.* (1988) Single-chain antigen-binding proteins. *Science* 242:423-426.

40. Wu H, Kwong PD, & Hendrickson WA (1997) Dimeric association and segmental variability in the structure of human CD4. *Nature* 387:527-530.

41. Hamburger ZA, Brown MS, Isberg RR, & Bjorkman PJ (1999) Crystal structure of invasin: a bacterial integrin-binding protein. *Science* 286:291-295.

42. Mrosek M, *et al.* (2007) Molecular determinants for the recruitment of the ubiquitin-ligase MuRF-1 onto M-line titin. *FASEB J* 21:1383-1392.

43. Cai Y, *et al.* (2008) Optimizing the codon usage of synthetic gene with QPSO algorithm. *J Theor Biol* 254:123-127.

44. Sandhu KS, Pandey S, Maiti S, & Pillai B (2008) GASCO: genetic algorithm simulation for codon optimization. *In Silico Biol* 8:187-192.

45. Shewmake TA, Solis FJ, Gillies RJ, & Caplan MR (2008) Effects of linker length and flexibility on multivalent targeting. *Biomacromolecules* 9:3057-3064.

46. Evers TH, van Dongen EM, Faesen AC, Meijer EW, & Merkx M (2006) Quantitative understanding of the energy transfer between fluorescent proteins connected via flexible peptide linkers. *Biochemistry* 45:13183-13192.

47. Yang X, Kurteva S, Ren X, Lee S, & Sodroski J (2005) Stoichiometry of envelope glycoprotein trimers in the entry of human immunodeficiency virus type 1. *J Virol* 79:12132-12147.